Magnetic polarization currents in double quantum dot devices

2003 J. Phys.: Condens. Matter 15 1147

(http://iopscience.iop.org/0953-8984/15/7/311)

INSTITUTE OF PHYSICS PUBLISHING JOURNAL OF PHYSICS: CONDENSED MATTER

J. Phys.: Condens. Matter **15** (2003) 1147–1154 PII: S0953-8984(03)54747-6

Magnetic polarization currents in double quantum dot devices

Sam Young Cho[1], Ross H McKenzie[1], Kicheon Kang[2] and Chul Koo Kim[3]

[1] Department of Physics, University of Queensland, Brisbane 4072, Australia
[2] Basic Research Laboratory, Electronics and Telecommunications Research Institute, Taejon 305-350, Korea
[3] Institute of Physics and Applied Physics, Yonsei University, Seoul 120-749, Korea

E-mail: sycho@physics.uq.edu.au

Received 14 October 2002
Published 10 February 2003
Online at stacks.iop.org/JPhysCM/15/1147

Abstract

We investigate coherent electron transport through a parallel circuit of two quantum dots (QDs), each of which has a single tunable energy level. Electrons tunnelling via each dot from the left lead interfere with each other at the right lead. It is shown that due to the quantum interference of tunnelling electrons the double QD device is magnetically polarized by coherent circulation of electrons on the closed path through the dots and the leads. By varying the energy level of each dot one can make the magnetic states of the device be *up*-, *non*- or *down*-polarized. It is shown that for experimentally accessible temperatures and applied biases the magnetic polarization currents should be sufficiently large to observe with current nanotechnology.

(Some figures in this article are in colour only in the electronic version)

The most interesting phenomena seen in mesoscopic electronic devices are due to the quantum coherence of electrons being maintained over a significant part of the transport process. Examples of such interference effects [1] that have been observed include weak localization, universal conductance fluctuations and Aharonov–Bohm (AB) oscillations. In 1995, Yacoby and co-workers [2] demonstrated the coherence of electron waves passing by resonant tunnelling through a quantum dot (QD) in a double-slit type interference in a ring geometry. Recent interference experiments [3–5] with two different transport paths in a ring geometry have enabled the realization of a phase sensitive probe of the effects of electron–electron interaction on the conductance oscillation such as Kondo correlations [5–9], as well as the anomalous phase of the transmission coefficients through a QD [10–15]. Two QDs have also been fabricated experimentally on two different electron pathways [16]. These double quantum dot (DQD) devices provide a good opportunity to test theories of resonant tunnelling [17, 18], cotunnelling [19–21] and many-body correlation effects [22, 23]. Compared with ballistic

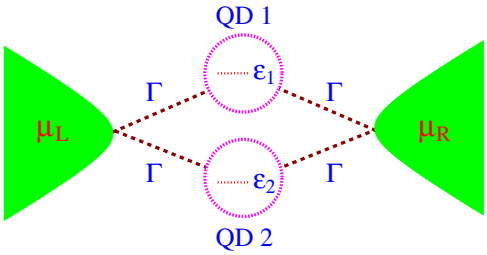

Figure 1. A DQD device. Both dots are tunnel-coupled to the left and right leads. The leads are characterized by the chemical potentials μ_L and μ_R. The tunnelling amplitudes between the dots and the leads are denoted by Γ. The energy level position in each dot is measured as ε_1 and ε_2 from the Fermi energy in the leads.

electron interference devices [24, 25], a DQD device makes it possible to manipulate the coherent tunnelling of electrons through each dot separately by varying the gate voltages of the dots. König and Gefen [21] have discussed quantum coherence in DQD devices with the *same* energy level in each dot.

We study coherent electron transport through two parallel QDs, each of which has a single *tunable* energy level (see figure 1). Remarkably, we find a coherent magnetic polarization current (MPC) circulating on the closed path connecting the dots and the leads as a function of each dot level position. This MPC is induced by coherent tunnelling for electron transport through each QD. We discuss the magnetic polarizability of the DQD device due to the MPC for finite temperature and finite applied bias.

We start with the model Hamiltonian

$$H = \sum_{\substack{k\in L,R \\ \sigma}} \varepsilon_k c^\dagger_{k\sigma} c_{k\sigma} + \sum_{\substack{i\in 1,2 \\ \sigma}} \varepsilon_i d^\dagger_{i\sigma} d_{i\sigma} + \sum_{\substack{i\in 1,2 \\ k\sigma\in L,R}} (V_{k,i} c^\dagger_{k\sigma} d_{i\sigma} + \text{h.c.}) \tag{1}$$

where $c_{k\sigma}$ and $d_{i\sigma}$ are the annihilation operators with spin σ for electrons in the leads and the dots ($i = 1, 2$) respectively. ε_1 and ε_2 are the level energies in each dot, measured relative to the Fermi energy of the leads. The symmetric tunnel-coupling between the dots and the leads will be assumed to be independent of energy, $|V_{k,i}| = |V|$.

In our interferometer, where the two electron pathways are allowed from one lead to the other lead, the levels of the dots are assumed not to be coupled to each other directly. Then we do not take into account direct interactions such as tunnel-coupling and Coulomb interactions between the two dots. Furthermore, to simplify the analysis and clarify the origin of the MPC in the interferometer the intradot electron–electron interaction is not taken into account. This allows us to obtain exact analytical results which show that the physical origin of the MPC is due to interference effects that are present for near resonant transport. Then the level spacing in each dot is larger than the applied bias and temperature because electrons transport through a single level in the dots. Although intradot Coulomb interactions are considered in the Coulomb blockade regime, the resonant transport could be well explained in the Hartree–Fock mean-field level where the energy level of the dots can be described by a simple shift of the interaction parameter. We acknowledge that in some real devices electron–electron interaction effects may need to be taken into account and their effect on the MPC needs to be investigated.

The current from the left lead to the dots is defined by $I = I_L = -ed\langle N_L\rangle/dt = (ie/\hbar)\langle[N_L, H]\rangle$, where $N_L = \sum_{k\sigma\in L} c^\dagger_{k\sigma} c_{k\sigma}$ is the total number of electrons in the left lead. We will employ the Keldysh non-equilibrium Green function technique to identify the local currents and discuss the MPC in non-equilibrium situations, i.e., at finite bias. The latter

cannot be described by a Kubo linear response treatment [26]. Using the Green function $G^{<}_{k\sigma,i\sigma}(t-t') \equiv \mathrm{i}\langle d^{\dagger}_{i\sigma}(t')c_{k\sigma}(t)\rangle$ which involves electron operators for the leads and for each dot, one can then use the Keldysh technique to obtain the current written as

$$I = -\frac{e}{h}\sum_{k\sigma\in L}\int \mathrm{d}\varepsilon\,[V_{k,1}G^{<}_{k\sigma,1\sigma}(\varepsilon) + \mathrm{h.c.}] - \frac{e}{h}\sum_{k\sigma\in L}\int \mathrm{d}\varepsilon\,[V_{k,2}G^{<}_{k\sigma,2\sigma}(\varepsilon) + \mathrm{h.c.}]. \tag{2}$$

The first (second) term of equation (2) describes electron transfer from the left lead to QD 1 (QD 2) or vice versa. Then each electron transfer can be defined as a local current through each dot, I_i. Thus the total current is the sum of the local currents through each dot, $I = I_1 + I_2$. If $V_{k,1} = 0$ ($V_{k,2} = 0$), equation (2) with a modified Green function gives the current through QD 2 (QD 1) in the absence of the other dot. The electron transfer from the lead to one of the dots can be a complex trajectory through the entire DQD device, as well as a direct tunnelling to the dot. The $G^{<}$ Green functions describe the current contributed by all Feynman paths going through each dot that start at one lead and end at the other lead. A similar identification of local currents was made previously [7]. With the Keldysh technique for nonlinear current through the system, the local currents through each dot are given by [27, 28]

$$I_i = \frac{e}{h}\sum_{\sigma}\int \mathrm{d}\varepsilon\,(f_L(\varepsilon) - f_R(\varepsilon))\mathcal{T}_i(\varepsilon), \tag{3}$$

where the local transmission spectral functions are defined by $\mathcal{T}_i(\varepsilon) = \{\Gamma^L \boldsymbol{G}^{\mathrm{r}}_{\sigma}(\varepsilon)\Gamma^R \boldsymbol{G}^{\mathrm{a}}_{\sigma}(\varepsilon)\}_{ii}$ which is the ith diagonal component of the matrix transmission spectral function. Here, $f_\alpha(\varepsilon) = f(\varepsilon - \mu_\alpha)$ is the Fermi–Dirac distribution function of the leads $\alpha = L, R$ and $\mu_L = -\mu_R = eV/2$ with applied bias eV between two leads. Due to tunnelling, each dot level acquires a finite line width $\Gamma = 2\pi|V|^2\mathcal{N}$, where $\mathcal{N}$ is the density of states in the leads. The matrix coupling to the leads is described by $\Gamma^L = \Gamma^R = \Gamma\begin{pmatrix} 1 & 1 \\ 1 & 1 \end{pmatrix}$. $\boldsymbol{G}^{\mathrm{r}}_{\sigma}(\varepsilon)$ is the matrix dot Green function defined in time space as $G^{\mathrm{r}}_{ij,\sigma}(t-t') = -\mathrm{i}\theta(t-t')\langle\{d_{i\sigma}(t), d^{\dagger}_{j\sigma}(t')\}\rangle$. By using the equation of motion treatment, one can obtain the matrix Green function of the dots as

$$\boldsymbol{G}^{\mathrm{r}}_{\sigma}(\varepsilon) = \begin{pmatrix} \varepsilon - \varepsilon_1 + \mathrm{i}\Gamma & \mathrm{i}\Gamma \\ \mathrm{i}\Gamma & \varepsilon - \varepsilon_2 + \mathrm{i}\Gamma \end{pmatrix}^{-1} \tag{4}$$

and $\boldsymbol{G}^{\mathrm{a}}_{\sigma}(\varepsilon) = [\boldsymbol{G}^{\mathrm{r}}_{\sigma}(\varepsilon)]^{\dagger}$. Accordingly, the local transmission spectral functions are written by

$$\mathcal{T}_1(\varepsilon) = \frac{\Gamma^2(\varepsilon - \varepsilon_2)(2\varepsilon - \varepsilon_1 - \varepsilon_2)}{(\varepsilon - \varepsilon_1)^2(\varepsilon - \varepsilon_2)^2 + (2\varepsilon - \varepsilon_1 - \varepsilon_2)^2\Gamma^2} \tag{5}$$

$$\mathcal{T}_2(\varepsilon) = \frac{\Gamma^2(\varepsilon - \varepsilon_1)(2\varepsilon - \varepsilon_1 - \varepsilon_2)}{(\varepsilon - \varepsilon_1)^2(\varepsilon - \varepsilon_2)^2 + (2\varepsilon - \varepsilon_1 - \varepsilon_2)^2\Gamma^2}. \tag{6}$$

Note that these can be negative. The total current is the sum of the current through each dot $I = I_1 + I_2$ which is just the current conservation. This leads to the total transmission spectral function as $\mathcal{T}(\varepsilon) = \mathcal{T}_1(\varepsilon) + \mathcal{T}_2(\varepsilon)$,

$$\mathcal{T}(\varepsilon) = \frac{\Gamma^2(2\varepsilon - \varepsilon_1 - \varepsilon_2)^2}{(\varepsilon - \varepsilon_1)^2(\varepsilon - \varepsilon_2)^2 + (2\varepsilon - \varepsilon_1 - \varepsilon_2)^2\Gamma^2}. \tag{7}$$

We note that this is always positive. The classical analogue of our system is two resistors in parallel. I_1 and I_2 must then both be positive. In contrast, in a quantum system the only constraint is that current conservation requires $I = I_1 + I_2$. It is not required that $I > I_1, I_2$. This was pointed out previously by Jayannavar and Deo [29] for the case of a metallic ring coupled to leads.

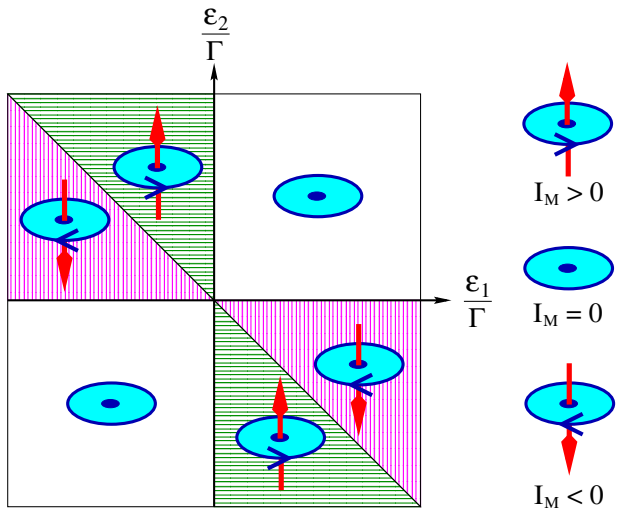

Figure 2. Magnetic polarization of the DQD device as a function of the energy level positions of each dot $(\varepsilon_1/\Gamma, \varepsilon_2/\Gamma)$, in the limit of zero applied bias at zero temperature for $\mu_R < \mu_L$. The vertical arrows stand for the magnetic moment of the DQD device whose length and direction depend on the amplitude and direction of the MPC respectively.

Let us assume the cases of $I < I_1$ or $I < I_2$ under current conservation for $\mu_R < \mu_L$. For given energy levels $(\varepsilon_1, \varepsilon_2)$, if $I(\varepsilon_1, \varepsilon_2) < I_1(\varepsilon_1, \varepsilon_2)$, we can assign an excess current $I_{exc}(\varepsilon_1, \varepsilon_2)$. Then we can rewrite the total current as $I(\varepsilon_1, \varepsilon_2) = I_1(\varepsilon_1, \varepsilon_2) - I_{exc}(\varepsilon_1, \varepsilon_2)$. The current conservation gives rise to the local excess current of $I_{exc}(\varepsilon_1, \varepsilon_2) = -I_2(\varepsilon_1, \varepsilon_2)$ which should circulate *clockwise* on the closed path through the dots and the leads. In the opposite case of $I < I_2$, the excess current becomes $I_{exc}(\varepsilon_1, \varepsilon_2) = -I_1(\varepsilon_1, \varepsilon_2)$ circulating *counter-clockwise* on the closed path. The circulating current makes the device magnetically polarized. Therefore, we define the circulating current as an MPC $I_M \equiv -I_{exc}$. We choose its direction for the case of $I < I_1$ as *positive*. It should be noted that this is purely a quantum coherent mesoscopic phenomenon.

Considering the transport current (TC), I, and MPC, I_M, on an equal footing, we define the MPC as

$$I_M = \frac{-e}{h} \sum_{\sigma} \int \mathrm{d}\varepsilon \, (f_L(\varepsilon) - f_R(\varepsilon)) \mathcal{T}_M(\varepsilon) \tag{8}$$

with the effective spectral function, $\mathcal{T}_M(\varepsilon)$. The $\mathcal{T}_M(\varepsilon)$ can be extracted from the following arguments. Let us recall the transmission spectral functions for $\varepsilon_1 < \varepsilon_2$. $\mathcal{T}(\varepsilon)$ has three extremum points, that is, $\mathcal{T}(\varepsilon_1) = \mathcal{T}(\varepsilon_2) = 1$ (resonant transmission) and $\mathcal{T}(\bar{\varepsilon}) = 0$ (anti-resonant transmission), where $\bar{\varepsilon} = (\varepsilon_1 + \varepsilon_2)/2$. At $\varepsilon = \bar{\varepsilon}$, the anti-resonance of $\mathcal{T}(\varepsilon)$ gives rise to a pronounced dip structure originating from the destructive interference between the transmissions through one QD and the other. Such an anti-resonant feature in a transport system with two different transmission channels is well understood as the Fano effect [30]. Next, the two local transmission spectral functions of $\mathcal{T}_1(\varepsilon)$ and $\mathcal{T}_2(\varepsilon)$ have three characteristic points, that is, $\mathcal{T}_1(\varepsilon_1) = 1$ [$\mathcal{T}_2(\varepsilon_2) = 1$] and $\mathcal{T}_1(\varepsilon_2) = \mathcal{T}_1(\bar{\varepsilon}) = 0$ [$\mathcal{T}_2(\varepsilon_1) = \mathcal{T}_2(\bar{\varepsilon}) = 0$]. These points have nothing to do with resonant and anti-resonant tunnelling through each dot. The two local transmission spectral functions only give us information about the local currents. Then we have to determine the behaviour of the local spectral functions in other energy regions. It is convenient to consider the ratio of the local transmission to the total transmission. The

ratios are written by $\mathcal{T}_1(\varepsilon)/\mathcal{T}(\varepsilon) = 1/(1+g(\varepsilon))$ and $\mathcal{T}_2(\varepsilon)/\mathcal{T}(\varepsilon) = 1/(1+g(\varepsilon)^{-1})$, where $g(\varepsilon) = (\varepsilon-\varepsilon_1)/(\varepsilon-\varepsilon_2)$. For $\varepsilon < \varepsilon_1$ and $\varepsilon > \varepsilon_2$, since $0 < g(\varepsilon) < 1$, the ratios are between 0 and 1. In these regions, there are no local excess currents. However, for $\varepsilon_1 < \varepsilon < \bar{\varepsilon}$, $\mathcal{T}_1(\varepsilon)/\mathcal{T}(\varepsilon) > 1$ [$\mathcal{T}_2(\varepsilon)/\mathcal{T}(\varepsilon) < 0$] and for $\bar{\varepsilon} < \varepsilon < \varepsilon_2$, $\mathcal{T}_1(\varepsilon)/\mathcal{T}(\varepsilon) < 0$ [$\mathcal{T}_2(\varepsilon)/\mathcal{T}(\varepsilon) > 1$]. These spectral properties give rise to the MPC at a given energy ε. Similarly, one can decide the $\mathcal{T}_M(\varepsilon)$ for $\varepsilon_1 > \varepsilon_2$. Consequently, we obtain the $\mathcal{T}_M(\varepsilon)$ in terms of the local transmission spectral functions as

$$\mathcal{T}_M(\varepsilon) = \sum_{i\neq j} \theta(\varepsilon_i - \varepsilon_j)\{\theta(\varepsilon-\bar{\varepsilon})\theta(\varepsilon_i-\varepsilon)\mathcal{T}_j(\varepsilon) - \theta(\varepsilon-\varepsilon_j)\theta(\bar{\varepsilon}-\varepsilon)\mathcal{T}_i(\varepsilon)\}. \tag{9}$$

Equations (8) and (9) are the central result of this work. Note that, for a given energy level position $(\varepsilon_1, \varepsilon_2)$ in each dot, the $\mathcal{T}_M(\varepsilon)$ is non-zero between the two energy levels $\varepsilon_i < \varepsilon < \varepsilon_j$ and is an anti-symmetric function with respect to $\bar{\varepsilon}$, $\mathcal{T}_M(\varepsilon-\bar{\varepsilon}) = -\mathcal{T}_M(\bar{\varepsilon}-\varepsilon)$. These properties of $\mathcal{T}_M(\varepsilon)$ determine the window of applied bias in which the MPC can be measured.

At zero temperature, the limit of zero applied bias is the simplest case. The TC is proportional to the transmission of incoming electrons at the Fermi energy ($\varepsilon_F = 0$); $\lim_{eV\to 0} I = (2e/h)\mathcal{T}(\varepsilon)|_{\varepsilon=\varepsilon_F} eV$ and the MPC becomes $\lim_{eV\to 0} I_M = (-2e/h)\mathcal{T}_M(\varepsilon)|_{\varepsilon=\varepsilon_F} eV$. Then the linear conductance $G = I/V$ shows that the resonances intersect each other due to interference effects when the dot energy levels ε_1 and ε_2 are varied. This agrees quantitatively with the experimental data in figure 2(a) of [16]. The MPC is also produced by interference effects. When the energy level of one dot is lying below the Fermi energy and that of the other is lying above the Fermi energy, the MPC appears to polarize the DQD device. If both energy levels of dots are below or above the Fermi energy the device is not magnetically polarized. This implies that the interference between the electron and hole channels produces the MPC. Figure 2 shows the magnetic polarization as a function of $(\varepsilon_1/\Gamma, \varepsilon_2/\Gamma)$ for $\mu_R < \mu_L$. It is shown that manipulating the energy level position of each dot, one can magnetize the DQD devices as *up*-, *non*-or *down*-polarized. Applying a finite bias between the leads, the properties of $\mathcal{T}_M(\varepsilon)$ change the polarization zone boundaries. A finite applied bias develops a *non*-polarization zone satisfying the conditions of $-eV/2 < |\varepsilon_1 - \varepsilon_2| < eV/2$ or $-eV/2 < \varepsilon_1, \varepsilon_2 < eV/2$. While the *up*-, and *down*-polarization zones are extended to the *non*-polarization zone of the limit of zero applied bias because the electron and hole channels near the Fermi energy within the window of the applied bias contribute to the MPC. It should be noted that when the applied bias is reversed to $\mu_R > \mu_L$ the magnetic moment of the device is reversed.

To illustrate the MPC for finite temperature, we choose a set of energy level positions $(\varepsilon_1/\Gamma, \varepsilon_2/\Gamma) = (0.3, -0.9)$ which can be adjusted to other values by varying the gate voltages. In fact, the level positions taken in the same polarization zone do not affect the physics of the MPC but only change its amplitude. We display the MPC and the TC as a function of applied bias for different temperatures in figure 3. As the applied bias increases from zero bias, both the TC and the MPC increase linearly. The MPC is always smaller than the TC for these given energy level positions. However, for the case of other energy level positions, the MPC can become larger than the TC (e.g. for $(\varepsilon_1/\Gamma, \varepsilon_2/\Gamma) = (0.5, -0.6)$, $I_M \simeq 5I$ at low temperatures). This linear behaviour of the MPC shows that the MPC emerges only in non-equilibrium. Further increase of applied bias results in the MPC approaching its maximum value. Eventually, disappearance of the MPC occurs when the window of the applied bias becomes larger than the range of ε for which $\mathcal{T}_M(\varepsilon)$ has a non-zero value ($-0.9 < \varepsilon < 0.3$). The inset of figure 3(b) shows that the TC increases nonlinearly as the applied bias increases. In addition, compared with the MPC, the TC is suppressed for biases smaller than $eV = 0.6\Gamma$ but enhanced for biases larger than $eV = 0.6\Gamma$ by thermal effects. This originates from the fact that $\mathcal{T}(\varepsilon)$ has a pronounced dip structure at $\bar{\varepsilon} = -0.3\Gamma$, due to the Fano effect. However,

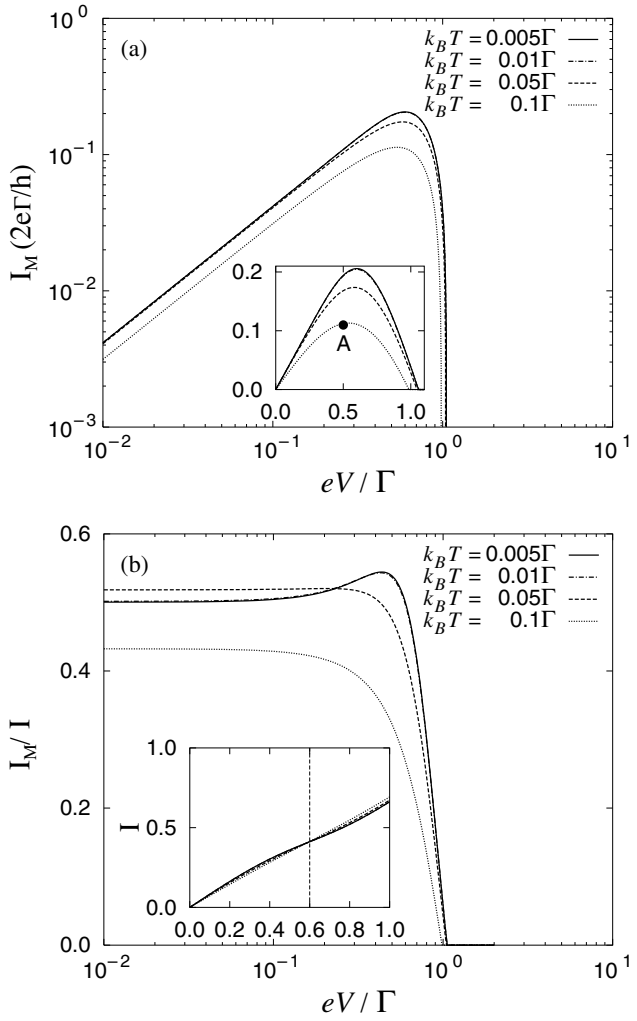

Figure 3. (a) MPC and (b) its ratio to the TC as a function of applied bias at $(\varepsilon_1/\Gamma, \varepsilon_2/\Gamma) = (0.3, -0.9)$ for various temperatures k_BT. In the insets, the currents are shown on a linear scale.

the anti-symmetric property of $\mathcal{T}_M(\varepsilon)$ gives rise to moderate thermal suppression of the MPC. The thermal suppression is manifestly shown in the temperature dependence of the MPC and the TC in figure 4. The relatively large applied bias leads to the large amplitude of the MPC. This is consistent with the linear behaviour of the MPC in the I_M–V curve. The insets of figures 4(a) and (b) show, compared with the TC, the more rapid suppression of the MPC since $\mathcal{T}_M(\varepsilon)$ is zero for low and high energies. At $k_BT \simeq 0.05\Gamma$, the MPCs at various applied biases begin to be suppressed by thermal effects. For temperatures higher than $k_BT \simeq 0.2\Gamma$, thermal effects wash out this novel quantum coherent phenomenon.

From the experimental parameters measured in [16]; $\Gamma \simeq 50\ \mu$eV and $\mathcal{A} = 2.52 \times 10^{-13}$ m^2, where $\mathcal{A}$ is a corresponding area to AB oscillation, we can estimate the amplitude of a MPC and an induced magnetic moment, $|\vec{\mu}_D| = \mathcal{A} \cdot I_M$. At the point A in the inset of figure 3(a), for $k_BT = 0.1\Gamma$ ($T \simeq 50$ mK), one can estimate $I_M \simeq 0.36$ nA, when $eV \simeq 25\ \mu$eV

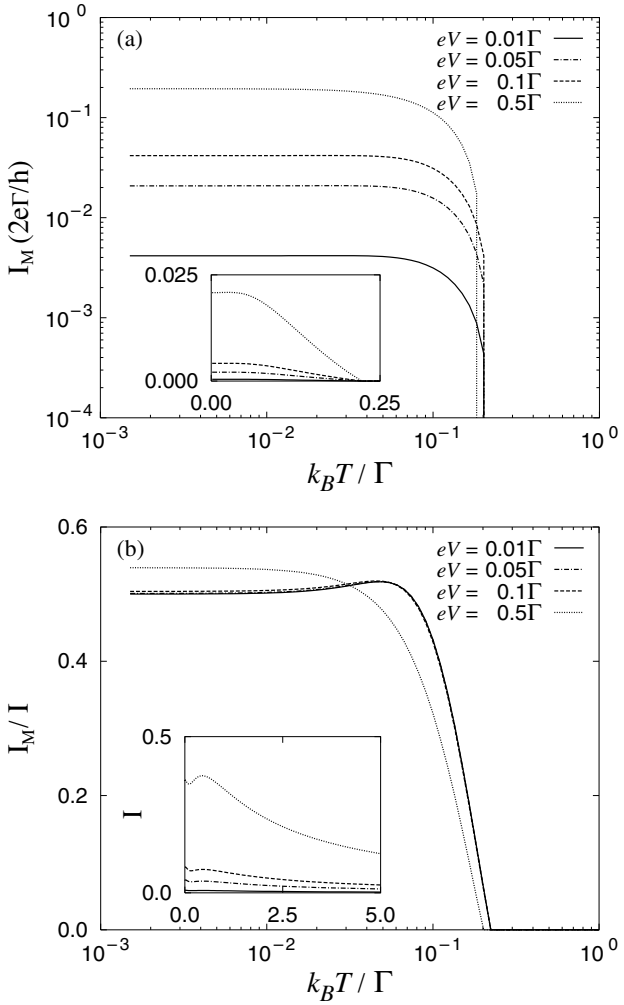

Figure 4. Temperature dependence of (a) the MPC and (b) its ratio to the TC at $(\varepsilon_1/\Gamma, \varepsilon_2/\Gamma) = (0.3, -0.9)$ for different values of the applied bias eV. In the insets, the currents are shown on a linear scale.

is applied. The induced magnetic moment of the device becomes $|\vec{\mu}_D| \simeq 9\ \mu_B$, where μ_B is the Bohr magneton. Comparison of this estimate of the MPC with recent measurements of persistent currents [25] suggests that the effects we are discussing can be observed with existing nanotechnology.

In summary, we studied coherent electron transport through two parallel QDs, each of which has a single tunable energy level. By changing these energy levels in the DQD device one can vary the *sign* and *magnitude* of the MPC induced by quantum interference effects. This current is sufficiently large that it should be experimentally observable.

Acknowledgments

This work was supported by the University of Queensland, the Australian Research Council, and the Korean Science and Engineering Foundation through the Center for Strongly Correlated

Materials Research (SNU). K Kang was supported by the National Research Laboratory Program of the Korean Ministry of Science and Technology.

References

[1] See, for a review
Imry Y 1997 *Introduction to Mesoscopic Physics* (New York: Oxford University Press)
Datta S 1995 *Electronic Transport in Mesoscopic Systems* (New York: Cambridge University Press)
[2] Yacoby A, Heiblum H, Mahalu D and Shtrikman H 1995 *Phys. Rev. Lett.* **74** 4047
[3] Schuster R, Buks E, Heiblum M, Mahalu D, Umansky V and Shtrikman H 1997 *Nature* **385** 417
[4] van der Wiel W G, De Franceschi S, Fujisawa T, Elzerman J M, Tarucha S and Kouwenhoven L P 2000 *Science* **289** 2105
[5] Ji Y, Heiblum M, Sprinzak D, Mahalu D and Shtrikman H 2000 *Science* **290** 779
[6] Gerland U, Delft J, Costi T A and Oreg Y 2000 *Phys. Rev. Lett.* **84** 3710
[7] Hofstetter W, König J and Schoeller H 2001 *Phys. Rev. Lett.* **87** 156803
[8] Kang K and Shin S-C 2000 *Phys. Rev. Lett.* **85** 5619
[9] Cho S Y, Kang K, Kim C K and Ryu C-M 2001 *Phys. Rev.* B **64** 033314
[10] Yeyati A L and Büttiker M 1995 *Phys. Rev.* B **52** R14360
[11] Hackenbroich G and Weidenmüller H A 1996 *Phys. Rev. Lett.* **76** 110
[12] Bruder C, Fazio R and Schoeller H 1996 *Phys. Rev. Lett.* **76** 114
[13] Ryu C-M and Cho S Y 1998 *Phys. Rev.* B **58** 3572
[14] Lee H-W 1999 *Phys. Rev. Lett.* **82** 2358
[15] Baltin R and Gefen Y 1999 *Phys. Rev. Lett.* **83** 5094
[16] Holleitner A W, Decker C R, Qin H, Eberl K and Blick R H 2001 *Phys. Rev. Lett.* **87** 256802
[17] Shahbazyan T V and Raikh M E 1994 *Phys. Rev.* B **49** 17123
[18] Kubala B and König J 2002 *Phys. Rev.* B **65** 245301
[19] Akera H 1993 *Phys. Rev.* B **47** 6835
[20] Loss D and Sukhorukov E V 2000 *Phys. Rev. Lett.* **84** 1035
[21] König J and Gefen Y 2001 *Phys. Rev. Lett.* **86** 3855
[22] Boese D, Hofstetter W and Schoeller H 2001 *Phys. Rev.* B **64** 125309
[23] Hofstetter W and Schoeller H 2002 *Phys. Rev. Lett.* **88** 016803
[24] Mailly D, Chapelier C and Benoit A 1993 *Phys. Rev. Lett.* **70** 2020
[25] Rabaud W, Saminadayar L, Mailly D, Hasselbach K, Benoit A and Etienne B 2001 *Phys. Rev. Lett.* **86** 3124
[26] Kubo R 1957 *J. Phys. Soc. Japan* **12** 570
[27] Meir Y and Wingreen N S 1992 *Phys. Rev. Lett.* **68** 2512
[28] Cho S Y, Kang K and Ryu C-M 1999 *Phys. Rev.* B **60** 16874
[29] Jayannavar A M and Deo P 1995 *Phys. Rev.* B **51** 10175
[30] Fano U 1961 *Phys. Rev.* **124** 1866